Chemical Engineering Communications
Publication details, including instructions for authors and subscription information:
http://www.informaworld.com/smpp/title~content=t713454788

MHD FREE CONVECTION FLOW OF A NANOFLUID PAST A VERTICAL PLATE IN THE PRESENCE OF HEAT GENERATION OR ABSORPTION EFFECTS

A. J. Chamkha[a]; A. M. Aly[b]
[a] Manufacturing Engineering Department, The Public Authority for Applied Education and Training, Shuweikh, Kuwait [b] Department of Mathematics, Faculty of Science, South Valley University, Qena, Egypt

Online publication date: 25 November 2010

To cite this Article Chamkha, A. J. and Aly, A. M.(2011) 'MHD FREE CONVECTION FLOW OF A NANOFLUID PAST A VERTICAL PLATE IN THE PRESENCE OF HEAT GENERATION OR ABSORPTION EFFECTS', Chemical Engineering Communications, 198: 3, 425 — 441
To link to this Article: DOI: 10.1080/00986445.2010.520232
URL: http://dx.doi.org/10.1080/00986445.2010.520232

Chem. Eng. Comm., 198:425–441, 2011

ISSN: 0098-6445 print/1563-5201 online
DOI: 10.1080/00986445.2010.520232

Taylor & Francis
Taylor & Francis Group

MHD Free Convection Flow of a Nanofluid past a Vertical Plate in the Presence of Heat Generation or Absorption Effects

A. J. CHAMKHA[1] AND A. M. ALY[2]

[1]Manufacturing Engineering Department, The Public Authority for Applied Education and Training, Shuweikh, Kuwait
[2]Department of Mathematics, Faculty of Science, South Valley University, Qena, Egypt

This work is focused on the numerical solution of steady natural convection boundary-layer flow of a nanofluid consisting of a pure fluid with nanoparticles along a permeable vertical plate in the presence of magnetic field, heat generation or absorption, and suction or injection effects. The model used for the nanofluid incorporates the effects of Brownian motion and thermophoresis. The governing boundary-layer equations of the problem are formulated and transformed into a non-similar form. The obtained equations are then solved numerically by an efficient, iterative, tri-diagonal, implicit finite-difference method. Comparisons with previously published work are performed and are found to be in excellent agreement. Representative results for the longitudinal velocity, temperature, and nanoparticle volume fraction profiles as well as the local heat transfer rates for various values of the physical parameters are displayed in both graphical and tabular forms.

Keywords Brownian motion; Heat generation/absorption; MHD; Nanofluid; Natural convection; Suction/injection; Thermophoresis

Introduction

Nanotechnology has been widely used in many industrial applications. This stems from the fact that materials with sizes of nanometers possess unique physical and chemical properties. A nanofluid is a term initially used by Choi (1995) and refers to a base liquid with suspended solid nanoparticles. Because traditional fluids used for heat transfer applications such as water, mineral oils, and ethylene glycol have a rather low thermal conductivity, nanofluids with relatively higher thermal conductivities have attracted enormous interest from researchers due to their potential in enhancement of heat transfer with little or no penalty in pressure drop. In their experimental work, Eastman et al. (1997) showed that an increase in thermal conductivity of approximately 60% can be obtained for a nanofluid consisting of water and 5 vol.% CuO nanoparticles. This is attributed to the increase in surface area due to the suspension of nanoparticles. Also, it was reported that a small

Address correspondence to A. J. Chamkha, Manufacturing Engineering Department, The Public Authority for Applied Education and Training, Shuweikh 70654, Kuwait. E-mail: achamkha@yahoo.com

amount (less than 1% volume fraction) of copper nanoparticles or carbon nanotubes dispersed in ethylene glycol or oil can increase their inherently poor thermal conductivity by 40% and 150%, respectively (Eastman et al., 2001; Choi et al., 2001). Das et al. (2003) reported a two- to four-fold increase in thermal conductivity enhancement for water-based nanofluids containing Al_2O_3 or CuO nanoparticles over a small temperature range, 21°–51°C. Keblinski et al. (2002) reported on the possible mechanisms of enhancing thermal conductivity. They showed that the Brownian motion of nanoparticles contributes much less than other factors such as the size effect, the clustering of nanoparticles, and the surface adsorption. The thermal conductivity enhancement of nanofluids was also observed by Masuda et al. (1993). The phenomenon of increased thermal conductivity of nanofluids suggests the possibility of using nanofluids in advanced nuclear systems (Buongiorno and Hu, 2005).

The effort to report theoretical models for nanofluid conductivity started immediately after the invention of nanofluids. Kumar et al. (2004) and Xue (2003) built simple analytical models that can explain the observed effect in nanofluids. However, such simple analytical models run into two problems. First, these models are based on certain assumptions of the heat transfer mechanism, and hence, they cannot shed light on complex mechanisms such as particle-particle and fluid-particle interactions. Second, they have certain adjustable constants that bring a certain amount of empiricism in the model, skirting the physics of the process. Hence, it is important to carry out large-scale simulations based on the fundamental principles to understand the physics of energy transport in nanofluids.

A comprehensive survey of convective transport in nanofluids was made by Buongiorno (2006), who gives an explanation for the abnormal increase of the thermal conductivity of nanofluids. After examining many mechanisms in the absence of turbulence, Buongiorno (2006) found that the Brownian diffusion and the thermophoresis effects are the most important and reported conservation laws for nanofluids in the presence of these two effects.

The problem of natural convection in a regular pure fluid past a vertical plate is a classical problem first studied theoretically by Pohlhausen in a contribution to an experimental study by Schmidt and Beckmann (1930) and later considered by Cheng and Minkowycz (1977). Exceptions are provided by the studies by Kuiken (1968, 1969). The situation was later clarified in the book by Bejan (1984). Khair and Bejan (1985) extended the problem of Cheng and Minkowycz (1977) to the case of heat and mass transfer. Studies on natural convection boundary-layer flow of nanofluids are very limited. Very recently, Kuznetsov and Nield (2010) and Nield and Kuznetsov (2009) studied the natural convective boundary-layer flow of a nanofluid past a vertical plate in the absence and presence of a porous medium using similarity solutions, respectively.

There has been a renewed interest in studying magnetohydrodynamic (MHD) flow and heat transfer due to the effect of magnetic fields on boundary-layer flow control and on the performance of many systems using electrically conducting fluids. In addition, this type of flow has attracted the interest of many investigators in view of its applications in many engineering problems such as MHD generators, plasma studies, nuclear reactors, and geothermal energy extractions. Several previous authors such as Raptis and Soundalgekar (1984), Agrawal et al. (1989), Jha and Singh (1990), Jha and Prasad (1992), Sattar (1994), Soundalgekar et al. (1995), and Singh et al. (2007) reported studies on MHD free convection and mass transfer flows.

In certain applications such as those involving heat removal from nuclear fuel debris, underground disposal of radioactive waste material, storage of food stuffs, and exothermic chemical reactions and dissociating fluids in packed-bed reactors, the working fluid heat generation or absorption effects are important. Representative studies dealing with heat generation or absorption effects have been reported previously by such authors as Acharya and Goldstein (1985), Vajravelu and Nayfeh (1992), and Chamkha (1997).

Recently, many articles concerning the study of MHD and heat and mass transfer effects have been published. El-Aziz (2010) studied the effect of chemical reaction on the flow and heat and mass transfer within a viscous fluid on an unsteady stretching sheet. Srinivas and Muthuraj (2010) examined the problem of MHD flow in a vertical wavy porous space in the presence of a temperature-dependent heat source with a slip-flow boundary condition. Abel et al. (2010) performed an analytical study for the problem of flow and heat transfer of an electrically conducting viscoelastic fluid over a continuously moving permeable stretching surface with nonuniform heat source/sink in a fluid-saturated porous medium. Maleque (2010) investigated the effects of mixed temperature- and depth-dependent viscosity and Hall current on unsteady flow of an incompressible electrically conducting fluid on a rotating disk in the presence of a uniform magnetic field. Ogulu and Makinde (2009) investigated the effect of thermal radiation absorption on unsteady free convective flow past a vertical plate in the presence of a magnetic field and constant wall heat flux. Abel and Begum (2008) studied the magnetohydrodynamic boundary-layer flow behavior and heat transfer characteristics of a viscoelastic fluid flow over a stretching sheet with radiation for the case of large Prandtl numbers.

The present work considers steady natural convection boundary-layer flow of a nanofluid along a permeable vertical plate in the presence of magnetic field, heat generation or absorption, suction or injection, Brownian motion of particles, and thermophoresis effects.

Mathematical Analysis

Consider two-dimensional steady MHD natural convection boundary-layer flow of a nanofluid consisting of an incompressible pure base fluid and nanoparticles along a semi-infinite vertical permeable plate in the presence of magnetic field, heat generation or absorption effects, particle Brownian diffusion, and thermophoresis effects. The x-axis is chosen along the vertical surface and the y-axis is taken normal to it. A transverse magnetic field of strength B_0 is applied parallel to the y-axis as shown in Figure 1. The magnetic Reynolds number is assumed small so the induced magnetic field is neglected. Possible fluid suction or injection is applied at the plate surface. The plate is maintained at a constant temperature and constant particle volume fraction.

The governing equations for this investigation are based on the balance laws of mass, momentum, thermal energy, and nanoparticles. Following Kuznetsov and Nield (2010) and employing the Oberbeck-Boussinesq approximation, these equations are written in dimensional form as

$$\nabla \cdot V = 0, \tag{1}$$

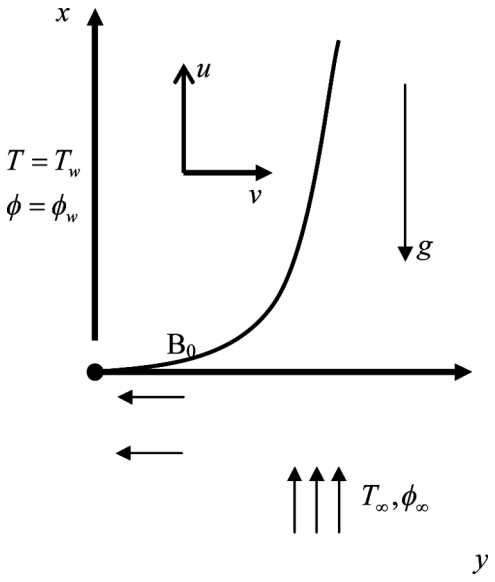

Figure 1. The physical model and coordinate system.

$$\rho_f(V \cdot \nabla V) = \mu(\nabla^2 V) - \nabla P + [\phi\rho_p + (1-\phi)(\rho_f\{1-\beta(T-T_\infty)\})]g - \sigma B_0^2 V, \quad (2)$$

$$(\rho C)_f(V \cdot \nabla T) = k\nabla^2 T + (\rho C)_p\left[D_B \nabla\phi \cdot \nabla T + \left(\frac{D_T}{T_\infty}\right)\nabla T \cdot \nabla T\right] + Q_0(T - T_\infty), \quad (3)$$

$$V \cdot \nabla\phi = D_B\nabla^2\phi + \left(\frac{D_T}{T_\infty}\right)\nabla^2 T. \quad (4)$$

Where $V = (u, v)$ is the fluid velocity vector, T is the fluid temperature, ϕ is the nanoparticle volume faction, P is the pressure, ρ_f is the material density of the base fluid, ρ_p is the material density of the nanoparticles, D_B and D_T are the Brownian diffusion coefficient and the thermophoresis diffusion coefficient, respectively, σ is the electrical conductivity of the base fluid, B_0 is the strength of the magnetic field, Q_0 is the heat generation or absorption coefficient such that $Q_0 > 0$ corresponds to heat generation while $Q_0 < 0$ corresponds to heat absorption, g is the acceleration due to gravity, μ, k, and β are the dynamic viscosity, thermal conductivity, and volumetric volume expansion coefficient of the fluid, respectively, $(\rho C)_f$ and $(\rho C)_p$are the heat capacity of the base fluid and the effective heat capacity of the nanoparticle material, respectively, and T_∞ is the free stream temperature. It should be noted that details of the derivation of Equations (3) and (4) are given in the articles by Buongiorno (2006) and Kuznetsov and Nield (2010) in the absence of magnetic field and heat generation or absorption effects.

The boundary conditions are as follows:

$$\begin{aligned} &u = 0, \quad v = v_w, \quad T = T_w, \quad \phi = \phi_w \quad \text{at } y = 0 \\ &u = v = 0, \quad T = T_\infty, \quad \phi = \phi_\infty \quad \text{as } y \to \infty \end{aligned} \quad (5)$$

By assuming that the nanoparticle concentration is dilute (that is, no particle-particle interaction exists) and using a suitable choice for the reference pressure, Equation (2) can be linearized and written as follows (Kuznetsov and Nield, 2010):

$$\rho_f(V\cdot\nabla V)=\mu(\nabla^2 V)-\nabla P+[(\rho_p-\rho_{f_\infty})(\phi-\phi_\infty)+(1-\phi_\infty)\rho_{f_\infty}\beta(T-T_\infty)]g-\sigma B_0^2 V \tag{6}$$

Using the standard boundary-layer approximation, based on a scale analysis, the governing equations can be written as

$$\frac{\partial u}{\partial x}+\frac{\partial v}{\partial y}=0, \tag{7}$$

$$\begin{aligned}\frac{\partial P}{\partial x}=\mu\frac{\partial^2 u}{\partial y^2}-\rho_f\left(u\frac{\partial u}{\partial x}+v\frac{\partial u}{\partial y}\right)\\ +[(1-\phi_\infty)\rho_{f_\infty}\beta g(T-T_\infty)-(\rho_p-\rho_{f_\infty})g(\phi-\phi_\infty)]-\sigma B_0^2 u\end{aligned} \tag{8}$$

$$\frac{\partial P}{\partial y}=0, \tag{9}$$

$$u\frac{\partial T}{\partial x}+v\frac{\partial T}{\partial y}=\alpha\nabla^2 T+\tau\left[D_B\frac{\partial\phi}{\partial y}\frac{\partial T}{\partial y}+\frac{D_T}{T_\infty}\left(\frac{\partial T}{\partial y}\right)^2\right]+\frac{Q_0}{(\rho C)_f}(T-T_\infty), \tag{10}$$

$$u\frac{\partial\phi}{\partial x}+v\frac{\partial\phi}{\partial y}=D_B\frac{\partial^2\phi}{\partial y^2}+\left(\frac{D_T}{T_\infty}\right)\frac{\partial^2 T}{\partial y^2}, \tag{11}$$

where $\alpha=\frac{k}{(\rho C)_f}$ is the base fluid thermal diffusivity and $\tau=\frac{(\rho C)_p}{(\rho C)_f}$ is the ratio of heat capacities.

Using cross differentiation to eliminate the pressure P and substituting the following dimensionless variables:

$$\begin{aligned}&\xi=x,\quad \eta=\frac{y}{x}Ra_x^{1/4},\quad u=\frac{\partial\psi}{\partial y},\quad v=-\frac{\partial\psi}{\partial x},\\ &S(\eta)=\frac{\psi}{\alpha Ra_x^{1/4}},\quad \theta=\frac{T-T_\infty}{T_w-T_\infty},\quad f=\frac{\phi-\phi_\infty}{\phi_w-\phi_\infty},\\ &Ra_x=\frac{(1-\phi_\infty)\beta g(T_w-T_\infty)x^3}{\nu\alpha}\end{aligned} \tag{12}$$

into Equations (7)–(11) yields the following non-similar equations:

$$S'''+\frac{1}{4\ \mathrm{Pr}}(3SS''-2S'^2)+\theta-Nr/f-M/S'-4\xi\left(S'\frac{\partial S'}{\partial\xi}-S''\frac{\partial S}{\partial\xi}\right)=0, \tag{13}$$

$$\theta''+\frac{3}{4}S\theta'+Nb\,f'\theta'+Nt\,\theta'^2+Q\theta+\xi\left(\theta'\frac{\partial S}{\partial\xi}-S'\frac{\partial\theta}{\partial\xi}\right)=0, \tag{14}$$

$$f''+\frac{3}{4}Le\ S\,f'+\frac{Nt}{Nb}\theta''+Le\xi\left(f'\frac{\partial S}{\partial\xi}-S'\frac{\partial f}{\partial\xi}\right)=0, \tag{15}$$

where $M=\frac{\sigma B_0^2x^2}{\mu Ra_x^{1/2}}$ and $Q=\frac{Q_0x^2}{\alpha(\rho C)_f Ra_x^{1/2}}$ are the magnetic field parameter and heat generation or absorption parameter, respectively. $\Pr=\frac{\nu}{\alpha}$ and $Le=\frac{\alpha}{D_B}$ are the Prandtl and Lewis numbers, respectively. $Nr=\frac{(\rho_p-\rho_{f\infty})(\phi_w-\phi_\infty)}{\rho_{f\infty}\beta(T_w-T_\infty)(1-\phi_\infty)}$, $Nb=\frac{(\rho C)_pD_B(\phi_w-\phi_\infty)}{(\rho C)_f\alpha}$, and $Nt=\frac{(\rho C)_pD_T(T_w-T_\infty)}{(\rho C)_f\alpha T_\infty}$ are the buoyancy ratio, the Brownian motion parameter, and the thermophoresis parameter, respectively.

The corresponding transformed dimensionless boundary conditions become:

$$S=S_w,\quad S'=0,\ \theta=1,\quad f=1,\quad \text{at } \eta=0$$

$$S'=0,\quad \theta=0,\quad f=0,\quad \text{at } \eta\to\infty \tag{16}$$

Of special significance for this type of flow and heat and mass transfer situation are the skin-friction coefficient, the Nusselt number Nu, and the Sherwood number Sh.

The wall shear stress τ_w, the surface heat flux q_w, and the surface mass flux m_w are defined as:

$$\tau_w=\mu\left.\frac{\partial u}{\partial y}\right|_{y=0}=\mu\alpha\frac{Ra_x^{3/4}\mu}{\xi^2}S''(\xi,0), \tag{17}$$

$$q_w=-k\left.\frac{\partial T}{\partial y}\right|_{y=0}=[-\theta'(\xi,0)](T_W-T_\infty)\frac{k}{\xi}Ra_x^{1/4}, \tag{18}$$

$$m_w=-D_B\left.\frac{\partial\phi}{\partial y}\right|_{y=0}=[-f'(\xi,0)](\phi_w-\phi_\infty)\frac{D_BRa_x^{1/4}}{\xi}, \tag{19}$$

Then the reduced local skin-friction coefficient, the reduced local Nusselt number, and the reduced local Sherwood number are given by:

$$\frac{Cf_x}{Ra_x^{3/4}}=\frac{\tau_w\xi^2}{\mu\alpha}=S''(\xi,0) \tag{20}$$

$$\frac{Nu_x}{Ra_x^{1/4}}=\frac{q_w\xi}{k(T_w-T_\infty)}=-\theta'(\xi,0) \tag{21}$$

$$\frac{Sh_x}{Ra_x^{1/4}}=\frac{m_w\xi}{(C_W-C_\infty)D_B}=-f'(\xi,0) \tag{22}$$

Numerical Method

The non-similar equations (13) through (15) are nonlinear and possess no analytical solution and must be solved numerically. The efficient, iterative, tri-diagonal, implicit finite-difference method discussed by Blottner (1970) has proven to be adequate for the solution of such equations. The equations are linearized and then discretized using three-point central difference quotients with variable step sizes in the η direction and using two-point backward difference formulas in the ξ direction with a constant step size. The resulting equations form a tri-diagonal system of algebraic equations that can be solved by the well-known Thomas algorithm (see Blottner, 1970). The solution process starts at $\xi = 0$, where Equations (13)–(15) are solved and then marches forward using the solution at the previous line of constant ξ until it reaches the desired value of ξ. Due to the nonlinearities of the equations, an iterative solution with successive over or under relaxation techniques is required. The convergence criterion required that the maximum absolute error between two successive iterations be 10^{-6}. The computational domain was made of 196 grids in the η direction and 101 grids in the ξ direction. A starting step size of 0.001 in the η direction with an increase of 1.0375 times the previous step size and a constant step size in the ξ direction of 0.01 were found to give very accurate results. The maximum value of η (η_∞), which represented the ambient conditions, was assumed to be 35. The step sizes employed were arrived at after performing numerical experimentations to assess grid independence and ensure accuracy of the results. The accuracy of the aforementioned numerical method was validated by direct comparisons with the numerical results reported earlier by Bejan (1984) and Kuznetsov and Nield (2010) for a regular fluid and in the absence of several effects. Table I presents the results of this comparison. It can be seen from this table that excellent agreement between the results exists. This favorable comparison lends confidence in the numerical results to be reported in the next section. It should be mentioned here that Kuznetsov and Nield (2010) used the same transformations in Equation (12) and reported similarity solutions corresponding to Equations (13)–(15) for $\xi = 0$. Their arrival at the self-similar equations was not understood until we solved the full non-similar equations (13)–(15) for which we found that there were no changes in the results as ξ changed for all parametric conditions. For this reason, all of the results to be reported subsequently correspond to the case $\xi = 0$.

Table I. Comparison of the reduced Nusselt number $Nu/Ra_x^{1/4}$ of a regular fluid for various values of Pr with $Le = 10$, $Nr = Nb = Nt = 10^{-5}$, $\mathrm{Sw} = 0$, $\mathrm{M} = 0$, and $\mathrm{Q} = 0$ with Bejan (1984) and Kuznetsov and Nield (2010)

Pr	Bejan (1984)	Kuznetsov and Nield (2010)	Present work
1	0.401	0.401	0.40178
10	0.465	0.463	0.4658
100	0.490	0.481	0.49063
1000	0.499	0.484	0.49739

Results and Discussion

In order to get a clear insight into the physical problem, numerical results are displayed with the help of graphical illustrations. The numerical computations were carried out for various values of the physical parameters such as the magnetic field parameter M, heat generation or absorption parameter Q, suction/injection parameter Sw, buoyancy ratio parameter Nr, Brownian motion parameter Nb, and the thermophoresis parameter Nt.

Figures 2–4 present the effects of the magnetic field parameter M on the longitudinal velocity, temperature, and nanoparticle volume fraction profiles, respectively. These figures are obtained for $\mathrm{Pr} = 0.025$, corresponding to liquid gallium metal. In general, application of a magnetic field has the tendency to slow down the movement of the fluid, causing its velocity close to the surface to decrease while it increases far downstream as the magnetic field parameter increases. The velocity profiles are characterized by distinctive peaks in the immediate vicinity of the wall, and as M increases these peaks decrease and move gradually downstream. In addition, this decrease in the flow movement as the magnetic field parameter M increases is accompanied by increases in the fluid temperature profiles and the nanoparticle volume fraction. These behaviors are clear from Figures 2–4.

Figures 5–7 show the effects of the Prandtl number Pr on the longitudinal velocity, temperature, and nanoparticle volume fraction profiles for two values of suction or injection parameter ($\mathrm{Sw} = 0$ and $\mathrm{Sw} = 0.5$), respectively. It is seen that increasing the Prandtl number leads to increases in the longitudinal velocity and decreases in both the fluid temperature and the nanoparticle volume fraction. In addition, all of the longitudinal velocity, temperature, and nanoparticle volume fraction profiles decrease as the suction or injection parameter Sw increases.

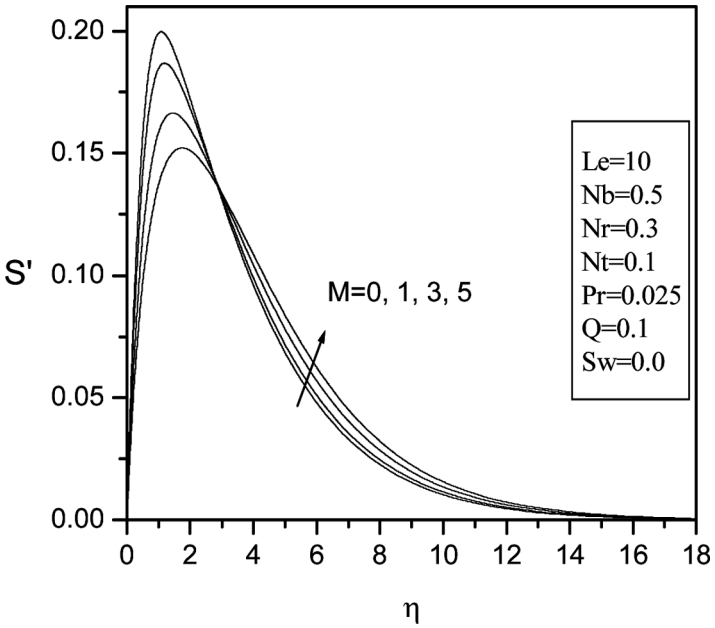

Figure 2. Effects of magnetic field parameter on the longitudinal velocity profiles.

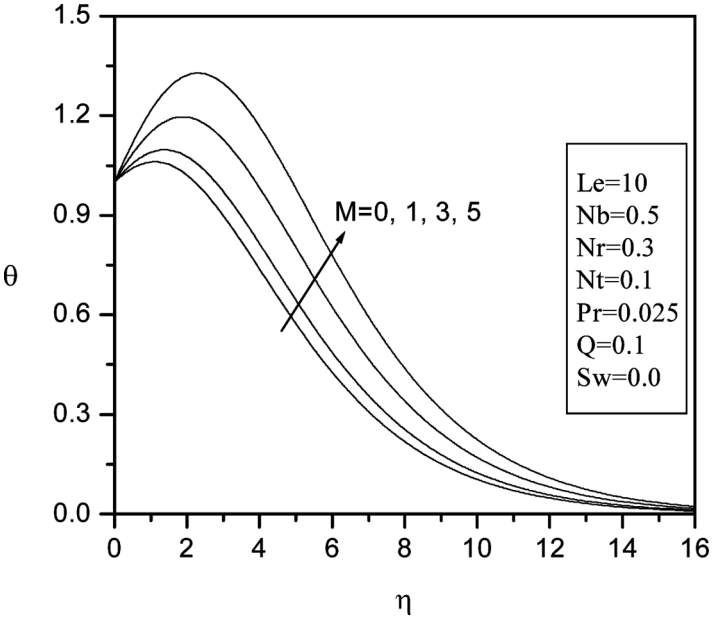

Figure 3. Effects of magnetic field parameter on the temperature profiles.

Figures 8–10 present the effects of the heat generation or absorption parameter Q on the longitudinal velocity, temperature, and nanoparticle volume fraction profiles, respectively. Increasing the heat generation or absorption parameter Q

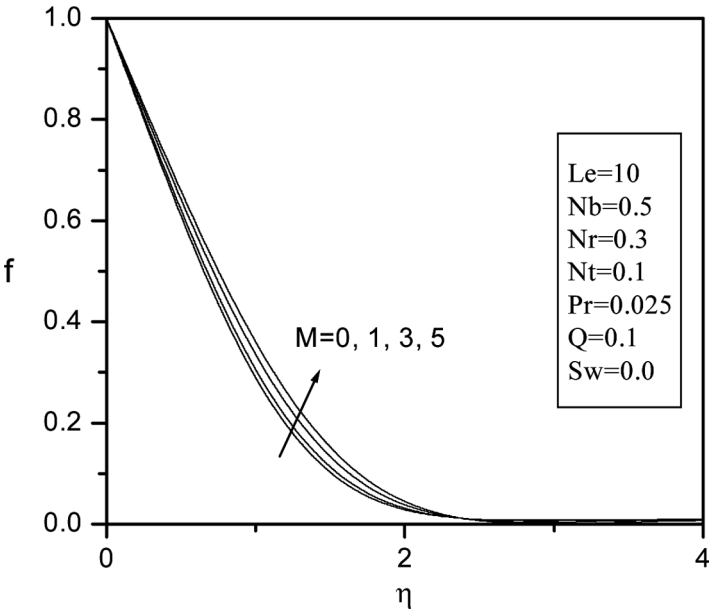

Figure 4. Effects of magnetic field parameter on the nanoparticle volume fraction.

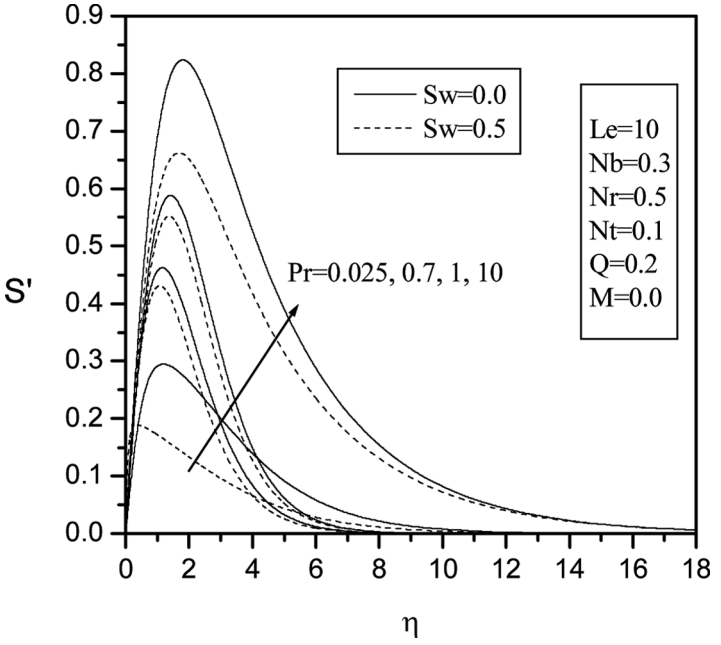

Figure 5. Effects of Prandtl number on the longitudinal velocity profiles.

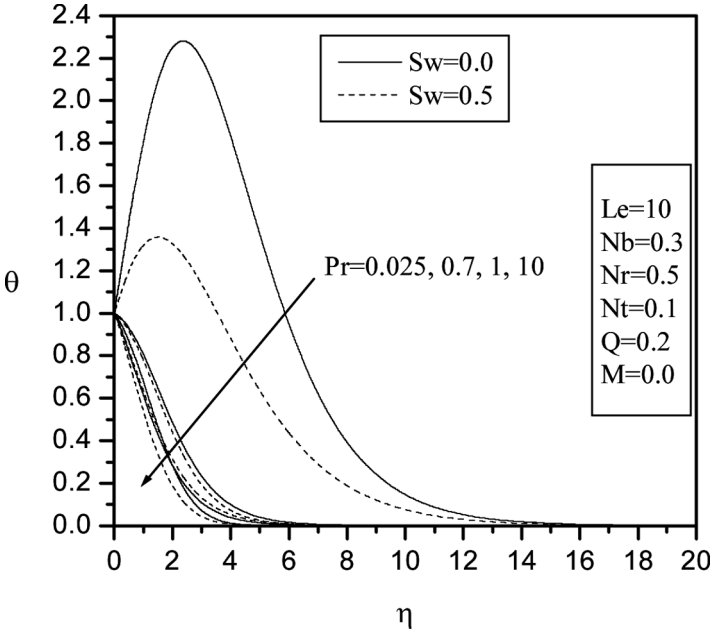

Figure 6. Effects of Prandtl number on the temperature profiles.

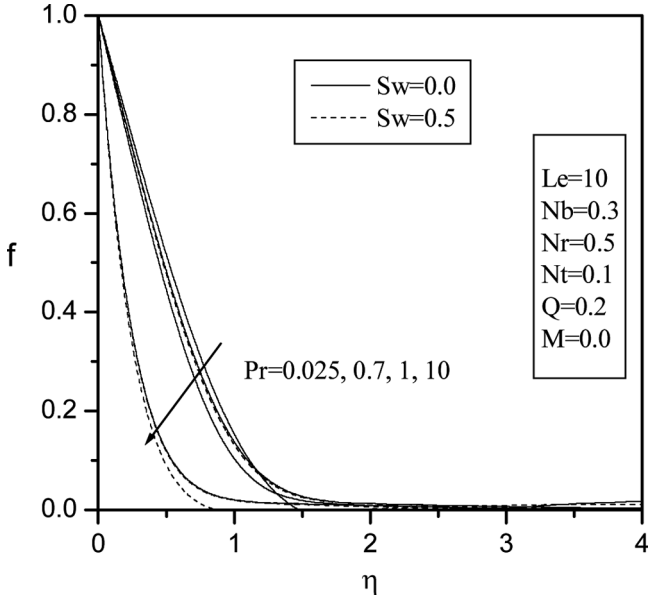

Figure 7. Effects of Prandtl number on the nanoparticle volume fraction.

has the tendency to increase the thermal state of the fluid. This increase in the fluid temperature causes more induced flow towards the plate through the thermal buoyancy effect. However, these increases in both the velocity and temperature profiles are accompanied by a slight decrease in the nanoparticle volume fraction profiles as the heat generation or absorption parameter increases.

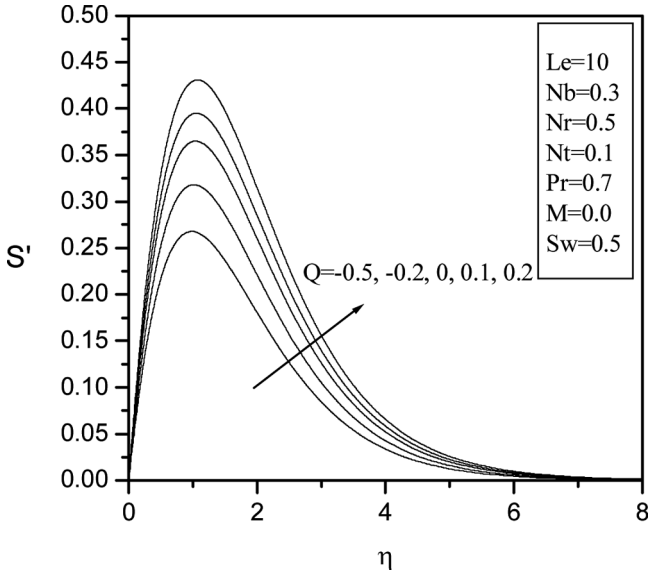

Figure 8. Effects of heat generation or absorption parameter on longitudinal velocity.

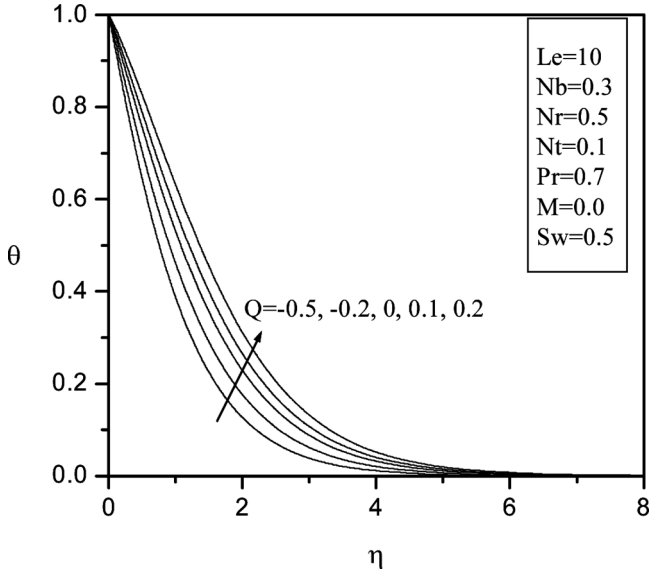

Figure 9. Effects of heat generation or absorption parameter on the temperature profiles.

Figures 11–13 predict the effects of the buoyancy ratio parameter Nr on the longitudinal velocity, temperature, and nanoparticle volume fraction profiles, respectively. It is seen that increasing the value of Nr leads to increases in the longitudinal velocity, temperature, and nanoparticle volume fraction profiles. These

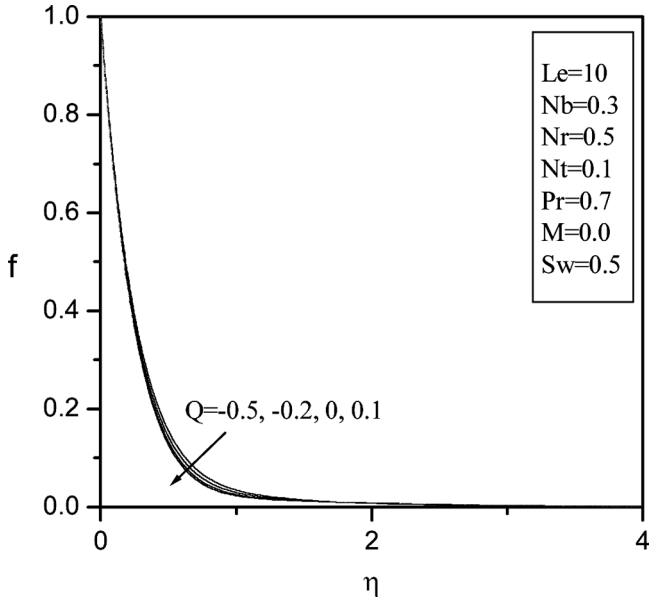

Figure 10. Effects of heat generation or absorption parameter on the nanoparticle volume fraction.

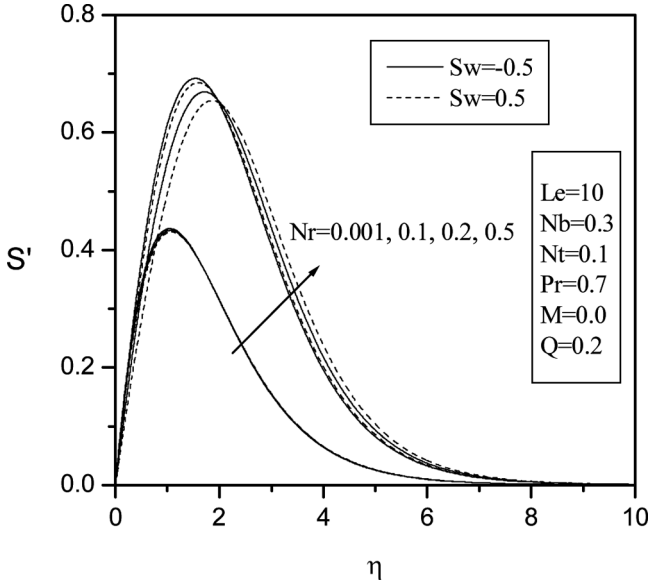

Figure 11. Effects of buoyancy ratio parameter on longitudinal velocity.

increases are due to the increased buoyancy effects. In addition, as the suction or injection parameter Sw increases from −0.5 to 0.5, it is observed that the longitudinal velocity decreases close to the wall while it increases downstream. However, both the temperature and nanoparticle volume fraction increase as Sw increases and these increases are accentuated as Nr increases.

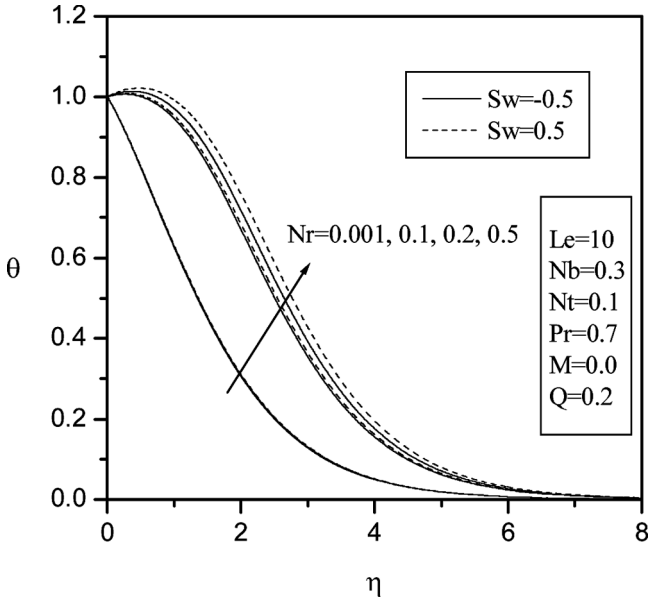

Figure 12. Effects of buoyancy ratio parameter on the temperature profiles.

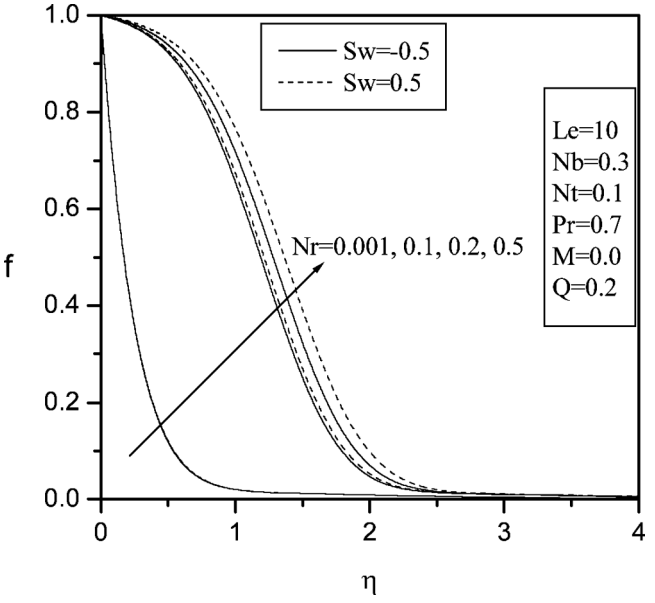

Figure 13. Effects of buoyancy ratio parameter on the nanoparticle volume fraction.

Table II presents the values of the reduced local skin-friction coefficient $Cf_x/Ra_x^{3/4}$, reduced local Nusselt number $Nu_x/Ra_x^{1/4}$, and the reduced local Sherwood number $Sh_x/Ra_x^{1/4}$ for different values of the buoyancy ratio Nr, Brownian motion parameter Nb, and thermophoresis parameter Nt. It is observed that the values of the reduced local skin-friction coefficient increase as the thermophoresis parameter Nt increases, while they decrease as either the buoyancy ratio Nr or the Brownian motion parameter Nb increases. Furthermore, the reduced local Nusselt number is predicted to decrease as either the buoyancy ratio Nr, Brownian motion

Table II. Values of the reduced local skin-friction coefficient, local Nusselt number, and local Sherwood number for various values of Nr, Nb, and Nt with Sw = −0.5, M = 0.0, Pr = 0.7, Le = 10, and Q = 0.2

Nr	*Nb*	*Nt*	$C/Ra_x^{3/4}$	$Nu/Ra_x^{1/4}$	$Sh/Ra_x^{1/4}$
0.001	0.3	0.1	0.9053885	−0.04942	0.0665
0.1			0.8546038	−0.05529	0.06235
0.3			0.7373396	−0.07062	0.054
0.5			0.6127617	−0.08873	0.04531
	0.01		0.6867313	−0.06238	0.5728996
	0.1		0.6081572	−0.0721	0.08039
	0.2		0.6088979	−0.0807	0.05368
	0.5		0.6216289	−0.1026294	0.03925
	0.3	0.001	0.6042188	−0.08361	0.02654
		0.01	0.6050050	−0.08411	0.02827
		0.2	0.6213040	−0.09286	0.06344

Table III. Values of the reduced local skin-friction coefficient, local Nusselt number, and local Sherwood number for various values of Sw, Le, Q, and M with Nr = 0.5, Nb = 0.3, and Nt = 0.1

Sw	*Le*	*Q*	*M*	$C/Ra_x^{3/4}$	$Nu/Ra_x^{1/4}$	$Sh/Ra_x^{1/4}$
−0.5	10	0.2	0	0.6127256	−0.08791	0.04543
0				0.8188518	0.08176	1.083785
0.5				0.9246035	0.2739808	3.993448
0	1			0.7066094	0.03507	0.4173937
	5			0.7873459	0.07321	0.8329982
	100			0.8990709	0.09679	2.468357
0.5	10	−0.5		0.6470249	0.7559673	3.764656
		−0.2		0.7347536	0.5868872	3.846617
		0		0.8148425	0.4487515	3.912705
		0.2		0.9245878	0.2746357	3.993286
0.0		0.1	0	0.4490116	−0.1039336	0.7999267
			3	0.3385836	−0.1875183	0.7294467
			5	0.2902568	−0.2496893	0.6942506

parameter Nb, or the thermophoresis parameter Nt increases. Moreover, the reduced local Sherwood number decreases as either the buoyancy ratio parameter or the Brownian motion parameter increases. On the other hand, the reduced local Sherwood number increases as the thermophoresis parameter increases.

Table III shows the values of $Cf_x/Ra_x^{3/4}$, $Nu_x/Ra_x^{1/4}$, and $Sh_x/Ra_x^{1/4}$ for different values of the suction/injection parameter Sw, Lewis number Le, heat generation or absorption parameter Q, and the magnetic field parameter M. It is seen that the reduced local skin-friction coefficient increases as either the suction/injection parameter, Lewis number, or heat generation or absorption parameter increases while it decreases as the magnetic field parameter increases. The reduced local Nusselt number increases as either the suction/injection parameter or the Lewis number increases. However, the reduced local Nusselt number decreases as either the heat generation or absorption parameter or the magnetic field parameter increases. Finally, the reduced local Sherwood number increases as either the suction/injection parameter, Lewis number, or heat generation or absorption parameter increases while it decreases as the magnetic field parameter increases.

Conclusions

This work considered steady natural convection boundary-layer flow of a nanofluid consisting of a pure fluid with nanoparticles along a permeable vertical plate in the presence of magnetic field, heat generation or absorption, and suction or injection effects. The pioneering model used for the nanofluid also incorporated the effects of particle Brownian motion and thermophoresis. The governing boundary-layer equations are formulated, nondimensionalized, and then transformed into a set of non-similarity equations that were solved numerically by an efficient, iterative, tri-diagonal, implicit finite-difference method. Comparisons with previously published work were made and the results were found to be in excellent agreement.

It was found that, in general, the local skin-friction coefficient increased as either the suction/injection parameter, thermophoresis parameter, Lewis number, or heat generation or absorption parameter increased, while it decreased as either the buoyancy ratio, Brownian motion parameter, or magnetic field parameter increased. Also, the local Nusselt number increased as either the suction/injection parameter or Lewis number increased while it decreased as either the buoyancy ratio, Brownian motion parameter, thermophoresis parameter, heat generation or absorption parameter, or magnetic field parameter increased. Furthermore, the local Sherwood number increased as either the thermophoresis parameter, suction/injection parameter, Lewis number, or heat generation or absorption parameter increased, whereas it decreased as either the buoyancy ratio, Brownian motion parameter, or magnetic field parameter increased. It was evident that the presence of nanoparticles in the pure fluid had clear effects on the heat and mass transfer characteristics.

References

Abel, M. S., and Begum, G. (2008). Heat transfer in MHD viscoelastic fluid flow on stretching sheet with heat source/sink, viscous dissipation, stress work, and radiation for the case of large Prandtl number, *Chem. Eng. Commun.*, **195**, 1503–1523.

Abel, M. S., Nandeppanavar, M. M., and Malkhed, M. B. (2010). Hydromagnetic boundary layer flow and heat transfer in viscoelastic fluid over a continuously moving permeable stretching surface with nonuniform heat source/sink embedded in fluid-saturated porous medium, *Chem. Eng. Commun.*, **197**, 633–655.

Acharya, S., and Goldstein, R. J. (1985). Natural convection in an externally heated vertical or inclined square box containing internal energy sources, *J. Heat Transfer*, **107**, 855–866.

Agrawal, A. K., Kishor, B., and Raptis, A. (1989). Effects of MHD free convection and mass transfer on the flow past a vibrating infinite vertical cylinder, *Wärme-Stöffubertrag.*, **24**, 243–250.

Bejan, A. (1984). *Convection Heat Transfer*, John Wiley, New York.

Blottner, F. G. (1970). Finite-difference methods of solution of the boundary-layer equations, *AIAA J.*, **8**, 93–205.

Buongiorno, J. (2006). Convective transport in nanofluids, *J. Heat Transfer*, **128**, 240–250.

Buongiorno, J., and Hu, W. (2005). Nanofluid coolants for advanced nuclear power plants, in *Proceedings of International Conference on Advances in Petrochemicals and Polymers, ICAPP '05, Seoul, May 15–19*, paper no. 5705.

Chamkha, A. J. (1997). Non-Darcy fully developed mixed convection in a porous medium channel with heat generation/absorption and hydromagnetic effects, *Numer. Heat Transfer*, **32**, 853–875.

Cheng, P., and Minkowycz, W. J. (1977). Free convection about a vertical flat plate embedded in a porous medium with application to heat transfer from a dike, *J. Geophys. Res.*, **82**, 2040–2044.

Choi, S. (1995). Enhancing thermal conductivity of fluids with nanoparticle, in *Developments and Applications of Non-Newtonian Flows, 1995*, eds. D. A. Siginer and H. P. Wang, 99–105, American Society of Mechanical Engineers, New York.

Choi, S. U. S., Zhang, Z. G., Yu, W., Lockwood, F. E., and Grulke, E. A. (2001). Anomalous thermal conductivity enhancement in nano-tube suspensions, *Appl. Phys. Lett.*, **79**, 2252–2254.

Das, S. K., Putra, N., Thiesen, P., and Roetzel, W. (2003). Temperature dependence of thermal conductivity enhancement for nanofluids, *J. Heat Transfer*, **125**, 567–574.

Eastman, J. A., Choi, S. U. S., Li, S., Thompson, L. J., and Lee, S. (1997). Enhanced thermal conductivity through the development of nanofluids, in: *Nanophase and Nanocomposite*

Materials II, eds. S. Komarneni, J. C. Parker and H. J. Wollenberger, pp. 3–11, Materials Research Society, Pittsburgh.

Eastman, J. A., Choi, S. U. S., Li, S., Yu, W., and Thompson, L. J. (2001). Anomalously increased effective thermal conductivities of ethylene glycol-based nano-fluids containing copper nano-particles, *Appl. Phys. Lett.*, **78**, 718–720.

El-Aziz, M. A. (2010). Unsteady fluid and heat flow induced by a stretching sheet with mass transfer and chemical reaction, *Chem. Eng. Commun.*, **197**, 1261–1272.

Jha, B. K., and Prasad, R. (1992). MHD free convection and mass transfer flow through a porous medium with heat source, *J. Math. Phys. Sci.*, **26**, 1–8.

Jha, B. K., and Singh, A. K. (1990). Soret effects on free convection and mass transfer flow in the Stokes problem for an infinite vertical plate, *Astrophys. Space Sci.*, **173**, 251–255.

Keblinski, P., Phillpot, S. R., Choi, S. U. S., and Eastman, J. A. (2002). Mechanisms of heat flow in suspensions of nano-sized particles (nanofluids), *Int. J. Heat Mass Transfer*, **45**(4), 855–863.

Khair, K. R., and Bejan, A. (1985). Mass transfer to natural convection boundary-layer flow driven by heat transfer, *J. Heat Transfer*, **107**, 979–981.

Kuiken, H. K. (1968). An asymptotic solution for large Prandtl number free convection, *J. Eng. Math.*, **2**, 355–371.

Kuiken, H. K. (1969). Free convection at low Prandlt numbers, *J. Fluid Mech.*, **39**, 785–798.

Kumar, D. H., Patel, H. E., Kumar, V. R. R., Sundararajan, T., Pradeep, T., and Das, S. K. (2004). Model for heat conduction in nanofluids, *Phys. Rev. Lett.*, **93**(14), 144301.

Kuznetsov, A. V., and Nield, D. A. (2010). Natural convective boundary-layer flow of a nanofluid past a vertical plate, *Int. J. Therm. Sci.*, **49**, 243–247.

Maleque, K. A. (2010). Effects of combined temperature- and depth-dependent viscosity and Hall current on an unsteady MHD laminar convective flow due to a rotating disk, *Chem. Eng. Commun.*, **197**, 506–521.

Masuda, H., Ebata, A., Teramae, K., and Hishinuma, N. (1993). Alteration of thermal conductivity and viscosity of liquid by dispersing ultra-fine particles, *Netsu Bussei*, **7**, 227–233.

Nield, D. A., and Kuznetsov, A. V. (2009). The Cheng–Minkowycz problem for natural convective boundary-layer flow in a porous medium saturated by a nanofluid, *Int. J. Heat Mass Transfer*, **52**, 5792–5795.

Ogulu, A., and Makinde, O. D. (2009). Unsteady hydromagnetic free convection flow of a dissipative and radiating fluid past a vertical plate with constant heat flux, *Chem. Eng. Commun.*, **196**, 454–462.

Raptis, A. A., and Soundalgekar, V. M. (1984). MHD flow past a steadily moving infinite vertical plate with mass transfer and constant heat flux, *Z. Angew. Math. Mech.*, **64**, 127–130.

Sattar, M. A. (1994). Free convection and mass transfer flow through a porous medium past an infinite vertical porous plate, *Indian J. Pure Appl. Math.*, **25**, 259–266.

Schmidt, E., and Beckmann, W. (1930). Das Temperatur-und Geschwindikeitsfeld von einer Wärme abgebenden senkrechten Platte bei natürlicher Konvection, II. Die versuche und ihre ergibnisse, *Forsch. Ingenieurwes.*, **1**, 391–406.

Singh, N. P., Singh, A. K., and Singh, A. K. (2007). MHD free convection and mass transfer flow past a flat plate, *Arab. J. Sci. Eng.*, **32**, 93–114.

Soundalgekar, V. M., Ray, S. N., and Das, U. N. (1995). MHD flow past an infinite vertical oscillating plate with mass transfer and constant heat flux, *Proc. Math. Soc.*, **11**, 95–98.

Srinivas, S., and Muthuraj, R. (2010). MHD flow with slip effects and temperature-dependent heat source in a vertical wavy porous space, *Chem. Eng. Commun.*, **197**, 1387–1403.

Vajravelu, K., and Nayfeh, J. (1992). Hydromagnetic convection at a cone and a wedge, *Int. Commun. Heat Mass Transfer*, **19**, 701–710.

Xue, Q. Z. (2003). Model for effective thermal conductivity of nanofluids, *Phys. Lett. A*, **307**, 313–317.